Check for updates

Ion-dependent structure, dynamics, and allosteric coupling in a non-selective cation channel

Adam Lewis[1], Vilius Kurauskas[1], Marco Tonelli[2] & Katherine Henzler-Wildman [1,2✉]

The selectivity filter (SF) determines which ions are efficiently conducted through ion channel pores. NaK is a non-selective cation channel that conducts Na^+ and K^+ with equal efficiency. Crystal structures of NaK suggested a rigid SF structure, but later solid-state NMR and MD simulations questioned this interpretation. Here, we use solution NMR to characterize how bound Na^+ vs. K^+ affects NaK SF structure and dynamics. We find that the extracellular end of the SF is flexible on the ps-ns timescale regardless of bound ion. On a slower timescale, we observe a structural change between the Na^+ and K^+-bound states, accompanied by increased structural heterogeneity in Na^+. We also show direct evidence that the SF structure is communicated to the pore via I88 on the M2 helix. These results support a dynamic SF with multiple conformations involved in non-selective conduction. Our data also demonstrate allosteric coupling between the SF and pore-lining helices in a non-selective cation channel that is analogous to the allosteric coupling previously demonstrated for K^+-selective channels, supporting the generality of this model.

[1] Department of Biochemistry, University of Wisconsin-Madison, Madison, WI 53706, USA. [2] National Magnetic Resonance Facility at Madison (NMRFAM), University of Wisconsin-Madison, Madison, WI 53706, USA. ✉email: henzlerwildm@wisc.edu

Bacterial ion channels are convenient model systems for understanding the structure, dynamics, and function of the pore domain of more complex eukaryotic channels. KcsA and MthK are two K+-selective, bacterial channels with homo-tetrameric pore structures. Each monomer is composed of two transmembrane helices, one pore helix, and the selectivity filter (SF), a structured loop with a highly conserved sequence that is responsible for selective K+ conduction[1–3]. This general architecture is conserved in eukaryotic voltage-gated K+ channels[4,5]. While much has been learned about conserved aspects of channel function from KcsA and MthK, these channels are K+-selective, potentially limiting insight into non-selective channels such as HCN, CNG, or TRP channels, which differ from K+ channels in SF structure[6,7]. NaK is a bacterial channel that non-selectively conducts both K+ and Na+. The structure of the NaK pore is very similar to KcsA and MthK (Fig. 1), differing only in the SF, where two of four canonical ion binding sites are abolished[8]. The biochemical tractability of systems like KcsA or NaK permits detailed biophysical studies aimed at understanding the fundamental and highly conserved processes of ion selectivity, permeation, and channel gating. In the present study, we employ NaK as a model non-selective channel to ask how the structure and dynamics of the SF are affected by ion identity and to what extent ion-dependent conformational changes in the SF are propagated throughout the pore.

In initial X-ray structures of NaK, the SF conformation was virtually unchanged when crystallized in 100 mM K+ or 500 mM Na+ (Fig. 1), leading to the hypothesis that K+ and Na+ bind in different modes to the same SF structure[8,9]. The limited number of ion binding sites in the non-selective SF reduces the frequency of knock-on ion interactions proposed to drive K+-selective conduction in 4-ion-binding site SF structures[10,11], thereby leading to non-selective conductance in NaK. However, MD simulations showed that the conformation of the NaK SF determined in 100 mM K+ (3E8H [https://doi.org/10.2210/pdb3E8H/pdb]) was not conductive to Na+, suggesting that the SF must change conformation to conduct Na+[12].

Indeed, several lines of evidence suggest that the NaK SF is flexible. An ssNMR and MD study[13] presented evidence that multiple SF states may be involved in Na+ permeation in NaK. SF residues V64 and G65 (Fig. 1) displayed ion-dependent chemical shifts, which was unexpected based on the identical conformation of these residues in Na+- and K+-bound crystal structures (Fig. 1). Na+ permeation was also not observed in MD simulations using the structure of NaK solved in 500 mM Na+ (3E83 [https://doi.org/10.2210/pdb3E83/pdb]), and only occurred when the SF was rendered asymmetric by flipping the T62 carbonyl orientation in a subset of subunits. Two subsequent crystallographic studies also revealed a degree of heterogeneity in the NaK SF. In one case, a micro-electron diffraction structure determined in Na+ (6CPV [https://doi.org/10.2210/pdb6CPV/pdb]) showed the N68 (Fig. 1) side chain could adopt multiple conformations[14]. In the second case, NaK was crystallized in mixed ion conditions in an alternate space group from earlier structures (6V8Y [https://doi.org/10.2210/pdb6V8Y/pdb])[15]. Both peptides in the asymmetric unit exhibited changes in backbone and side-chain structure in the region D66-S70. Collectively, these data suggest that the NaK SF is not static, and that structural heterogeneity in the SF on a relatively slow timescale may be important for achieving non-selective conductance of Na+ in addition to K+.

The structure of the SF in certain channels is also affected by allosteric coupling to the inner gate, and vice versa. Perhaps the most extensively characterized example is that of C-type inactivation in KcsA, where prolonged opening of the inner gate causes the SF to enter a 'collapsed' state that is non-conductive[16–20].

Recently, it has also been proposed that SF-inner gate coupling controls activation for MthK and KcsA[21,22]. In this model, the SF is non-conductive when the inner gate opening is small, but upon further opening the SF widens to allow permeation. Residues on M2 at the base of the SF mediate inter-gate coupling, specifically I100 and F103 for KcsA and I84 in MthK (analogous to I100 in KcsA). Upon prolonged opening, the KcsA SF undergoes a conformational change that results in inactivation. MthK has also been reported to inactivate, although the inactivation phenotype differs in MthK and KcsA[19,22–25]. Additionally, allosteric coupling between M2, the SF, and pore helix was observed via ssNMR to mediate the anionic lipid-induced opening of KirBac1.1[26]. Collectively, these data suggest that coupling between the SF and M2 may be an important, general regulator of ion channel conductance properties.
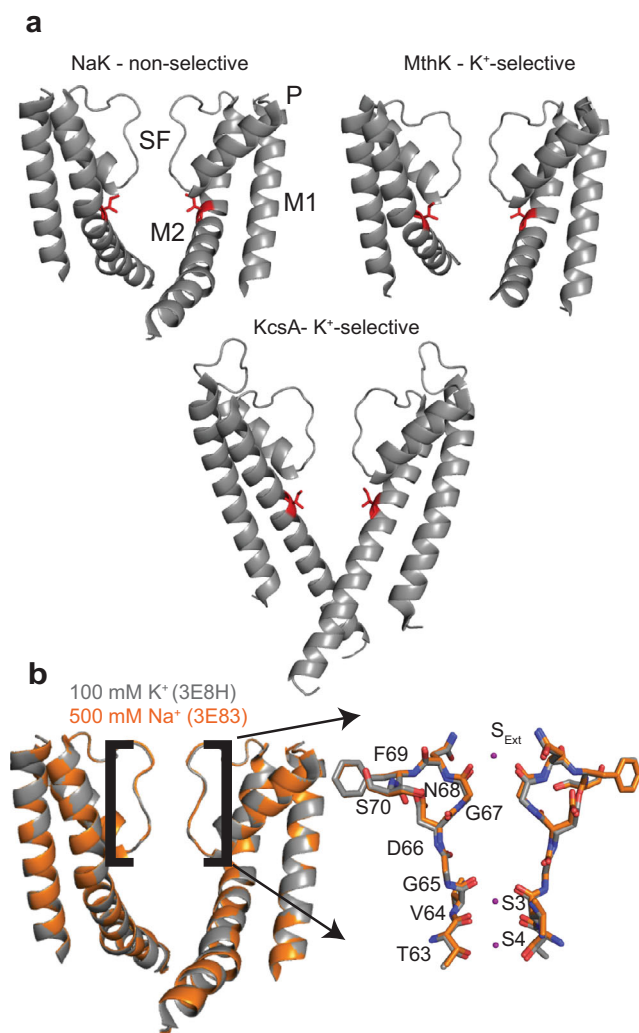

Fig. 1 NaK channel structural comparisons. a Structures and selectivities of 3 bacterial ion channels, NaK (3E8H [10.2210/pdb3E8H/pdb]), MthK (3LDC [10.2210/pdb3LDC/pdb]), and KcsA (1K4C [10.2210/pdb1K4C/pdb]). The selectivity filter (SF) along with M1, P, and M2 helices are labeled for NaK. Residue I88, I84, and I100 is highlighted in red on NaK, MthK, and KcsA structures respectively. **b** Overlay of NaK structures determined in 100 mM K+ (3E8H [10.2210/pdb3E8H/pdb]) and 500 mM Na+ (3E83 [10.2210/pdb3E83/pdb]). The SF along with M1, P, and M2 helices are labeled. The SF is enlarged on the right with residue labels. Ion binding sites are labeled and K+ ions modeled in the 3E8H [10.2210/pdb3E8H/pdb] structure are shown as well. In both panels, two opposing of four total subunits are shown for clarity.

Here we experimentally determine how the NaK SF structure changes to accommodate Na^+ vs. K^+ and how SF dynamics are affected by the permeant ion on both fast (ps-ns) and slow (ms-s) timescales. Solid-state NMR data indicates V64 and G65 adopt ion-dependent structural states, but resonances were not observed for residues 66-70[13] so it remains unclear how this region of the SF is affected by the permeant ion. We also assess whether the coupling mechanism observed in MthK and KcsA is also observed in NaK. Previously, our group has shown that NaK and NaK2K, a K^+-selective mutant of NaK with a different SF structure[27], have distinct NMR chemical shifts for residues far from the sites of mutation in the SF[28]. This demonstrates that in principle the state of the putative inner gate can be influenced by the structure of the SF. Indeed, initial MD data presented for NaK2K suggests that the SF and M2 helix are coupled in a similar manner to KcsA or MthK[22]. In ssNMR spectra of NaK, however, peaks for residues below V91 on M2 were not visible[13], making it impossible to assess how or if the SF structure is communicated throughout the pore in the wild-type channel.

Here we use solution NMR to investigate the ion dependence (Na^+ vs. K^+) of SF structure, dynamics, and coupling to the inner gate in NaK solubilized in isotropic bicelles ($q = 0.33$ DMPC/ DHPC). For these studies, we used a NaK construct lacking the first 18 residues. A very similar construct lacking the first 19 residues (NaKΔ19) has been used extensively in studies of ion selectivity in NaK[8,9,27,29,30] (referred to as NaK throughout for clarity). Our solution NMR-based approach allows us to observe resonances throughout the NaK structure and characterize dynamics in a quantitative manner. Using ^{15}N R_1, $R_{1\rho}$, and {^1H}-^{15}N NOE experiments, we show that residues 66–70 in the SF are highly dynamic on the ps-ns timescale regardless of bound ion. On a slower timescale, we observe chemical shift perturbations (CSPs) throughout the SF indicative of an ion-dependent conformational change that extends to the extracellular mouth. We also find evidence for increased structural heterogeneity in Na^+. Several SF residues exhibit multiple resonances in Na^+, while methyl-CPMG experiments show that V64 experiences pronounced chemical exchange on the low ms timescale. Further, CSPs far from the SF suggest that the SF structure may be coupled to the rest of the pore. Methyl-methyl NOEs show that the I88 side-chain, a residue critical for allosteric coupling in MthK and KcsA, adopts a different conformation in K^+ vs. Na^+.

Results

NaK SF flexibility differs markedly from the intracellular to extracellular end. To understand the impact of binding of Na^+ and K^+ on the structure and dynamics of the NaK channel, ^1H–^{15}N TROSY-HSQC spectra of U-^{15}N,^2H labeled NaK were collected in 100 mM K^+ and 600 mM Na^+. The high Na^+ concentration was chosen to saturate Na^+-binding to NaK in order to drive the SF towards a Na^+-preferred state, and is based on previously reported Na^+ binding constants determined by ITC[29]. Quantitative NMR studies of a protein the size of NaK solubilized in a bicelle require perdeuteration. In both ionic conditions, backbone amide resonances for residues 33-40, 53-65, and 79-87 are either weak or not visible due to lack of back-exchange of amide deuterons to protons after expression in D_2O (Supplementary Fig. 1). In order to monitor amides throughout NaK, we developed an SDS-based unfolding/refolding protocol to enhance the back-exchange of amide protons (See Methods, Supplementary note 1). Spectra of refolded NaK solubilized in isotropic bicelles overlay very well with spectra of NaK that did not undergo the refolding protocol, but the peak intensity is increased for many weak peaks in the K^+ sample and many more peaks are visible in the Na^+ sample (Supplementary Fig. 1). Thus, our SDS

back-exchange method did not alter the conformation of NaK, but does allow us to observe and assign nearly all backbone amides, enabling detailed investigation of NaK structure and dynamics.

With more backbone amides in the SF visible in the NMR spectrum as a result of our new purification scheme, we noticed that SF residues V64 and G65 were poorly back-exchanged in both ionic conditions, suggesting that these amides are not water-accessible. Conversely, intense resonances were observed for residues 66–70 at the mouth of the SF, leading us to hypothesize that the dynamic character of the SF differs along the pore axis. We performed ^{15}N R_1, $R_{1\rho}$, and {^1H}-^{15}N NOE measurements[31] using refolded samples in both 100 mM K^+ and 600 mM Na^+ to more quantitatively characterize ps-ns timescale internal dynamics in NaK (Supplementary note 2, Fig 2, Supplementary Data 1). R_1 and NOE data are shown in Fig. 2. For folded proteins with little internal motion, these quantities are consistent for residues in stable secondary structure, with the precise value depending on the global tumbling of the protein molecule (or in our case, protein plus bicelle). Indeed, measured R_1, R_2, and NOE values are quite uniform for residues predicted to be α-helical based on the crystal structure, suggesting that NaK remains well-ordered in our NMR samples (Fig. 2, Supplementary Fig. 2). Deviations from the average value for helical residues are indicative of the presence of internal dynamics, with increased R_1 values and decreased NOE values indicating enhanced dynamics[31,32].

It is clear that in both K^+ and Na^+ there is a pronounced gradient in ps-ns dynamics from the intracellular to extracellular end of the SF. Parameter values for V64 and G65 are similar to those for residues found in the transmembrane helices. V64 contributes to the canonical S3 and S4 binding sites, while G65 is adjacent to S3, and based on our relaxation data it is likely that these sites are stably maintained in solution. Conversely, there is a pronounced drop in the NOE and increase in R_1 from residues 66–70, indicating that the backbone in this region is more flexible than at the intracellular end of the SF. In particular, residues 67-69 have very elevated R_1 values and markedly lower NOE values indicative of extensive ps-ns timescale dynamics at these sites. The dynamic profile of the SF obtained here is generally consistent with crystallographic B factors for 3E8H [https://doi.org/10.2210/pdb3E8H/pdb] (100 mM K^+) and 3E83 [https://doi.org/10.2210/pdb3E83/pdb] (500 mM Na^+), which are elevated for residues 66-70 relative to V64 and G65[9]. B factors in this region are similar between 3E8H [https://doi.org/10.2210/pdb3E8H/pdb] and 3E83 [https://doi.org/10.2210/pdb3E83/pdb], which is consistent with our data showing similar ps-ns dynamics in K^+ and Na^+.

Our observation of elevated R_1 and NOE values at the extracellular mouth of the SF is in contrast to trends in R_1 and NOE values observed for KcsA solubilized in SDS micelles[33]. R_1 and NOE values were uniforms across the entire KcsA SF, consistent with a relatively rigid filter with minimal motions on the ps-ns timescale. Although the KcsA data were acquired in detergent, this offers the most direct comparison of the same type of NMR relaxation data that we have acquired for NaK in lipid bicelles. Our data indicate that the NaK SF is more flexible than the K^+-selective KcsA SF, especially around the S1/S2 ion binding sites in KcsA, which are replaced by a wider vestibule in NaK (Fig. 1). In particular, G67 in NaK (analogous to G79 in KcsA) exhibits relaxation parameters indicative of enhanced ps-ns dynamics that are absent in KcsA. Residues in KcsA analogous to N68-S70 in NaK were not analyzed due to signal overlap or low signal to noise[33]. Previous crystallographic studies of NaK proposed that the SF structure is stabilized by a hydrogen bond between the D66 side chain and N68 backbone amide[9]. We
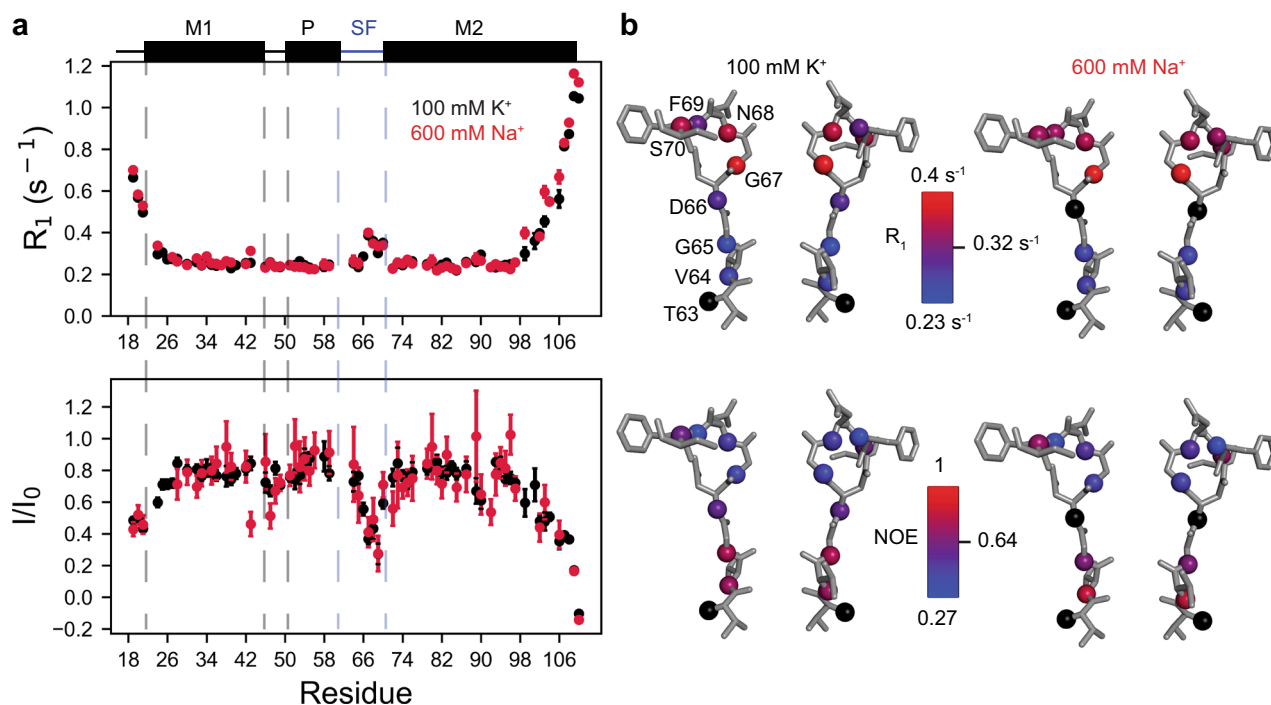
Fig. 2 Gradient in ps-ns dynamics across NaK SF. a Backbone amide ^{15}N R_1 and $\{^1H\}$–^{15}N NOE values recorded at 750 MHz for NaK in 100 mM K$^+$ (black) and 600 mM Na$^+$ (red). Secondary structure elements are shown above, where helices are rectangles and loops are lines. The boundaries between elements are based on the 3E8H [10.2210/pdb3E8H/pdb] crystal structure. Residues 63–70 are indicated by the blue lines and are shown as sticks in (**b**). Error bars were calculated as the SD of 500 Monte Carlo simulations, as described in the Methods. Note that the error in R_1 is smaller than the marker for the majority of residues. **b** Relaxation data plotted on the NaK SF (showing 2 of 4 opposing subunits). Backbone N atoms are shown as spheres and are colored according to the scale indicated for each parameter. Residues for which data are unavailable due to resonance overlap or lack of assignment are colored black.

observe low NOE values for N68, 0.43 ± 0.07 in K$^+$ and 0.49 ± 0.14 in Na$^+$, much lower than the observed NOE values for amides hydrogen-bonded in α-helices, suggesting that the interaction between D66 and N68 may be weaker than initially thought. Interestingly, subsequent crystal structures of NaK[14,15] showed both backbone and side-chain conformational changes for D66 and N68, consistent with our interpretation that the SF structure is labile in the region of D66-S70.

We have shown that not only is the NaK SF dynamic on a slow timescale, as shown previously by ssNMR[13], it is also dynamic on a fast timescale. This conclusion is consistent with our H/D exchange data showing that residues 66-70 more readily exchange with bulk water (Supplementary Fig. 1) and with the fact that correlations were not observed for residues 66-70 in dipolar-coupling based ssNMR experiments where motion impedes magnetization transfer[13,34]. Thus, our data clearly demonstrates that the extracellular mouth of the SF is structurally labile, potentially enabling this region to adapt to different types of bound ions.

The SF conformation is ion-dependent. Chemical shifts measured for NaK in Na$^+$ and K$^+$ were compared to further understand how ion identity affects the SF structure on a slower (ms-s) timescale. Backbone amide ^1H and ^{15}N chemical shifts were obtained from 2D TROSY-HSQC spectra while C' and Cα chemical shifts were obtained from TROSY-HNCO and HNCA spectra respectively. Additionally, ILV methyl chemical shifts were obtained from ^1H–^{13}C HMQC spectra of U-[^2H,^{15}N] Ile(δ1)-$^{13}CH_3$, Leu/Val-($^{13}CH_3$/$^{12}C^2H_3$) labeled NaK. Overlays of 2D TROSY-HSQC and ^1H–^{13}C HMQC spectra obtained in Na$^+$ and K$^+$ are shown in Supplementary Fig. 3.

Residues 64–70 in the SF region experience significant amide chemical shift perturbations (CSPs) between 100 mM K$^+$ and 600 mM Na$^+$ (Fig. 3, Supplementary Data 2). This is not due simply to a change in ionic strength (Supplementary Fig. 4, Supplementary Note 3), but reflects the difference in ion identity. Significant perturbations to Cα chemical shifts also occur for resides 66 and 68–70 while all residues in this region other than N68 exhibit perturbations to C' greater than 0.2 ppm. Chemical shift differences between K$^+$ and Na$^+$ could in principle result from changes in ion occupancy/coordination for residues in close proximity to the ion-binding sites, or from a structural change in this region. While carbonyl oxygen atoms are the ion-coordinating ligands in the SF, of the residues 66–70 only G67 C' is observed to bind ions in the crystal structures, at a site termed S_{ext} at the extracellular mouth (Fig. 1)[8,9]. The backbone carbonyls of D66 and N68 have been reported to bind ions at a site S_{side} in MD simulations[13]. A density assigned to a Na$^+$ ion was also resolved at this site in another recently published crystal structure[15]. The extent of backbone CSPs in the SF beyond these residues are difficult to explain solely based on changes in ion occupancy. Additionally, CSPs are observed for the methyl groups of V64, V59, L48, and I84, located behind the SF. Together, the extent of observed CSPs supports the existence of an ion-dependent conformational change in the SF, with residues 65-70 adopting distinct structural states in 100 mM K$^+$ and 600 mM Na$^+$.

Furthermore, several residues in the SF region have multiple resonances. More residues display additional resonances in Na$^+$ than in K$^+$, indicating a greater number of states in Na$^+$-saturated NaK. No peak doubling is observed in amide spectra in K$^+$, but spectra collected in Na$^+$ display minor resonances for G67, F69, and S70. These three residues undergo large CSPs upon changing
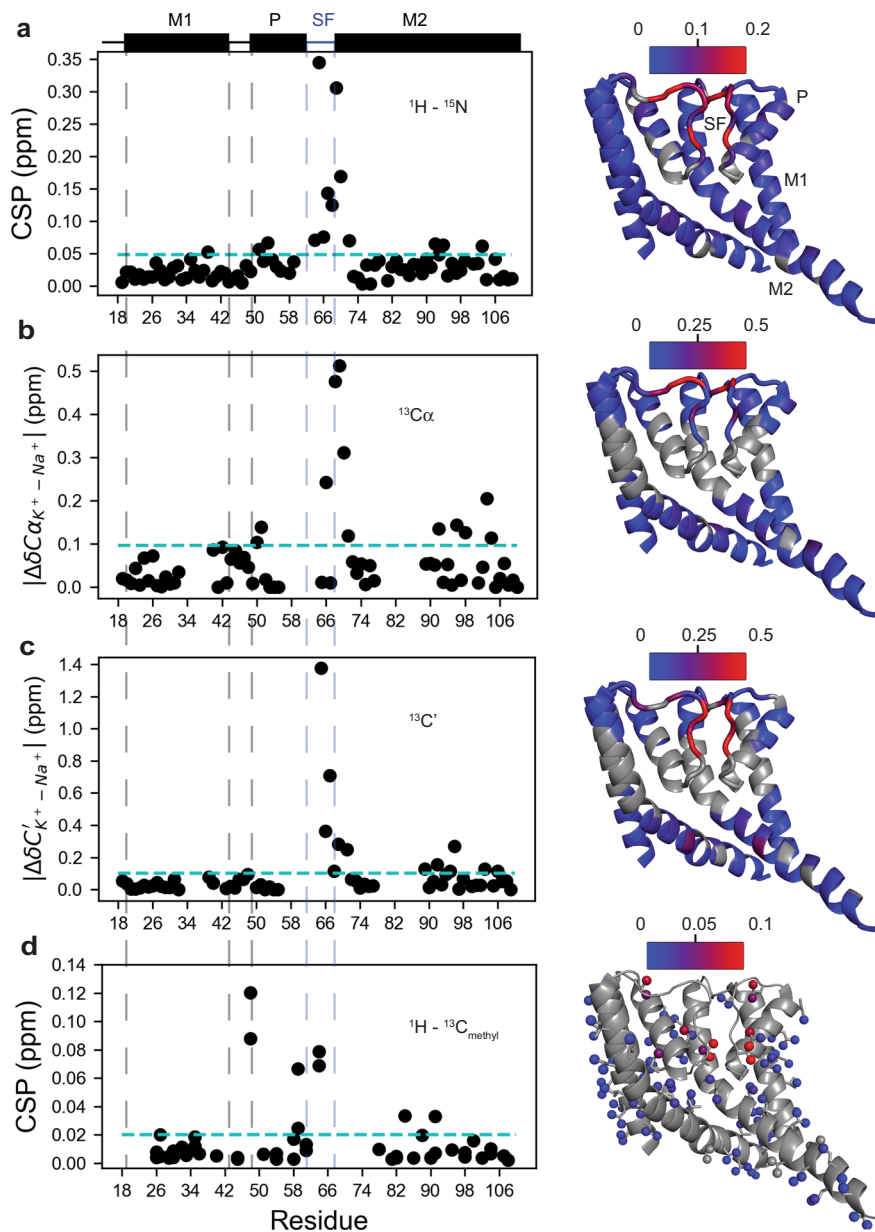
Fig. 3 SF and hinge residues display ion-dependent chemical shifts. Backbone amide (**a**) and ILV methyl (**d**) chemical shift perturbations (CSPs) along with $^{13}C'$ (**c**) and $^{13}C\alpha$ (**b**) chemical shift differences ($\Delta\delta$) were calculated for NaK in 100 mM K$^+$ vs 600 mM Na$^+$. CSPs (calculated as described in Methods) and $\Delta\delta$ values for residues assigned in both conditions are plotted against residue number. In each plot, the cyan line indicates 1.5σ above the 10% trimmed mean. CSPs and $\Delta\delta$ values are also plotted on the NaK structure (3E8H [10.2210/pdb3E8H/pdb], 2 adjacent of 4 subunits shown for clarity). Color scale bars are shown for each plot. ^{1}H–^{15}N CSPs, $^{13}C'$ $\Delta\delta$, and $^{13}C\alpha$ $\Delta\delta$ values are plotted on the backbone and residues for which data are not available are colored gray. ^{1}H–$^{13}C_{methyl}$ CSPs are plotted on the side-chains and the backbone is shown in gray. Secondary structure elements are indicated on the plots and labeled on the structure in panel **a**.

ionic conditions (Fig. 4). The γ1 and γ2 methyl groups of V64 and V59 are each split into two partially overlapped resonances in Na$^+$, while only a single resonance is observed in K$^+$ (Fig. 4). L48 δ methyl groups display at least two resonances in both ionic conditions. Interestingly, the major state for L48b is inverted between K$^+$ and Na$^+$. In K$^+$, the major state occurs at ~0.3 ppm in ^{1}H and has a population of ~86% while the minor peaks around 0.4 and 0.2 ppm have populations of ~7% each. In Na$^+$, the major state occurs at ~0.2 ppm, and has a population of ~82%. Only a single minor state is observed in this case. L48a displays three resonances in both ionic conditions. In K$^+$, again, the major state makes up 86% of the population while each minor state is ~7%;

however, the populations in Na$^+$ are more evenly distributed with populations of 47%, 37%, and 16%.

Collectively, these data indicate that SF adopts distinct states in K$^+$ and Na$^+$. The backbone CSP data suggest a structural change occurs in the SF at the extracellular mouth between residues 65–70, and methyl CSPs for residues 64, 59, and 84 suggest that the change in structure is propagated in the vicinity of the SF. The data also indicate that several minor SF states exist in Na$^+$. The CSPs we observe in the vicinity of the SF upon switching ion are largely consistent with very recent ssNMR data reported for NaK in liposomes[34], further emphasizing that the structure and dynamics of NaK are essentially the same in bicelles and liposomes. Next, we
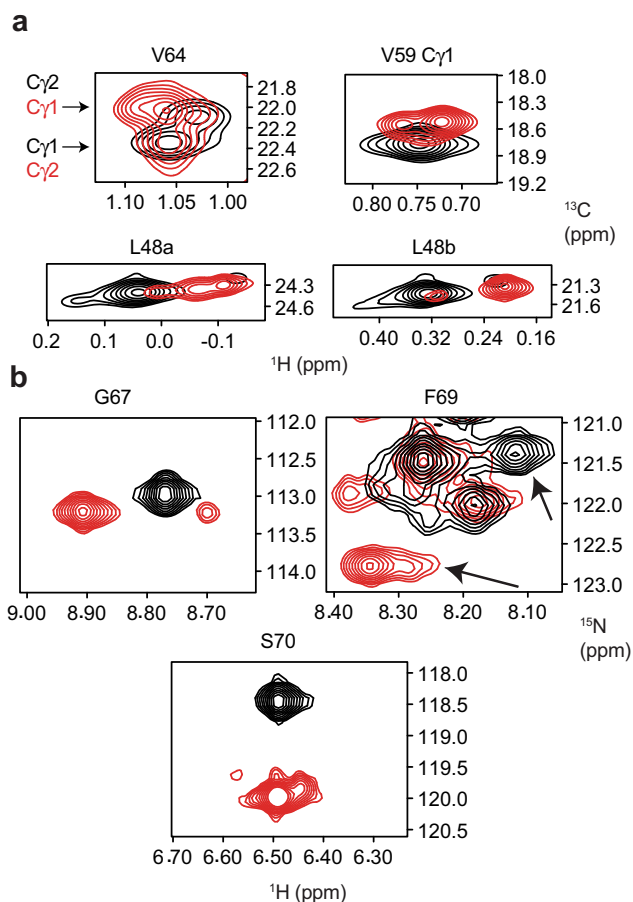
Fig. 4 Na+ increases heterogeneity in the selectivity filter. Overlays of selectivity filter (SF) peaks from (**a**) ^{1}H–^{13}C HMQC and (**b**) TROSY-HSQC spectra of NaK in 600 mM Na$^+$ (red) and 100 mM K$^+$ (black). Stereospecific assignments based on NOESY data are given where possible.

Fig. 5 I88 side chain conformation is ion dependent. a Strips for I88 Cδ1 from 3D CCH NOESY experiments collected in 600 mM Na$^+$ (red, ^{1}H ppm = 0.567) and 100 mM K$^+$ (black, ^{1}H ppm = 0.576). **b** Distances from I88 Cδ1 to V64 Cγ2 and V91 Cγ1 in the 'up' (black) and 'down' (red) conformations. NOESY data collected in K$^+$ is consistent with the 'up' conformation, while the data collected in Na$^+$ is more consistent with the 'down' conformation.

turned to methyl NOESY and CPMG experiments to more precisely and quantitatively characterize ion-dependent changes in NaK structure and slow-timescale dynamics.

The M2 helix is coupled to the SF. Structural coupling between the SF and the inner gate is frequently observed in K$^+$-selective channels and structurally related channels, such as NaK. Do the structural changes in the SF we detect in Na$^+$ versus K$^+$ propagate through the M2 helix? The first piece of evidence for structural coupling is that, while the largest CSPs occur near the SF, there are more subtle but still significant perturbations for residues at or below the hinge point that occurs around G87 on M2 (Fig. 3, Supplementary Data 2) Notably, significant CSPs are observed for the F92 amide, an aromatic residue that packs against the base of the SF and is known to regulate the NaK conductance[8]. Additional backbone CSPs are observed near the hinge; G89 C' and L90 H-N shift significantly between Na$^+$ and K$^+$. In methyl spectra, a perturbation is also evident for V91 Cγ1. These chemical shift perturbations may reflect a reorientation of the F92 side-chain between Na$^+$ and K$^+$ conditions, since ring currents can significantly impact chemical shifts. Significant backbone CSPs were also observed further down M2 at Q103 near the bundle crossing proposed to be the cytoplasmic gate of NaK[35,36]. In this region, a significant CSP is also observed for a methyl resonance ambiguously assigned to either V100 or V102 (Supplementary Fig. 3).
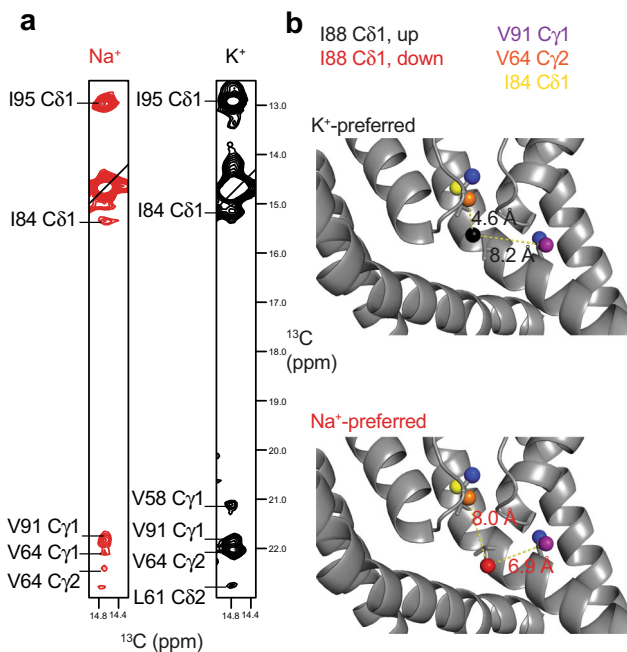
Methyl-methyl NOESY data was collected on ILV labeled NaK samples in K$^+$ and Na$^+$ to more directly assess potential conformational changes in M2. In general, NOE patterns for both samples are consistent with the overall architecture of NaKΔ19 observed in crystal structures, suggesting that potential conformational changes in M2 are most likely not large. It is clear, though, that the side chain of I88 adopts a different conformation in K$^+$ vs. Na$^+$ (Fig. 5). This is interesting because I88 is located in M2 at a position analogous to I100 in KcsA and I84 in MthK, two residues implicated in inter-gate allosteric coupling[19,22–24]. The I88 δ1 NOEs to V64 γ2 and I84 δ1 are much stronger in K$^+$ than Na$^+$. In addition, I88 δ1 has a stronger NOE to V91 γ1 than V64 γ2 in Na$^+$, while the relative intensities of these two NOEs are reversed in K$^+$. In crystal structures of NaK, the shortest predicted intermethyl distance for I88 δ1 is to I95, consistent with our observation of a strong NOE to I95 under both conditions. In the structure of NaK in 100 mM K$^+$ (3E8H [https://doi.org/10.2210/pdb3E8H/pdb]), the I88 side chain is modeled in two conformations, one with Cδ pointing up and one with Cδ pointing down; whereas in the 3E83 [https://doi.org/10.2210/pdb3E83/pdb] structure of NaK in 500 mM Na$^+$, I88 is only modeled in the down conformation. In the down conformation, I88 δ1 is closer to V91 γ1 than V64 γ2, consistent with the observed NOE intensities in Na$^+$. Our data are therefore consistent with I88 adopting the down conformation in Na$^+$ and the up conformation in K$^+$.

Recently reported ssNMR data supported ion-dependent structural changes in NaK solely in the vicinity of the SF[34]. In ssNMR spectra of NaK, resonances are not observed for residues 91–110, making it impossible to conclude how this region is affected by the permeant ion. Because we can resolve resonances throughout the NaK structure, we see that residues in the M2 helix show CSPs indicative of a structural change between the
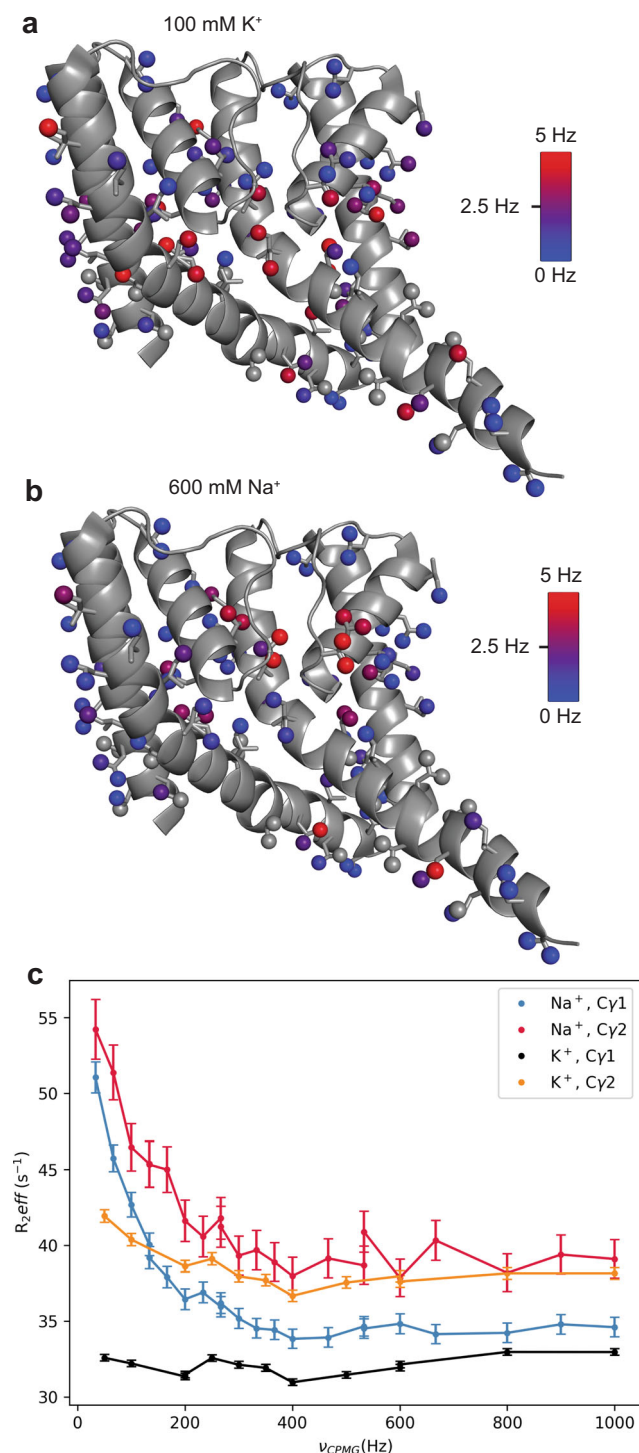
Fig. 6 V64 undergoes enhanced chemical exchange in the presence of Na⁺. a ^{13}C Multiple Quantum (MQ) R_{ex} values for ILV labeled NaK in the presence of K⁺ (**a**) and Na⁺ (**b**) are plotted on the structure (3E8H [10.2210/pdb3E8H/pdb]). **c** ^{13}C MQ relaxation dispersion curves for V64 in the presence of 100 mM K⁺ and 600 mM Na⁺. Error bars represent the SD from three replicated data points.

Na⁺- and K⁺-bound states. Additionally, we are not limited to observing changes in backbone structure because of our methyl-labeling approach. Indeed, we can see that methyl resonances for V59 in the P helix and I84, I88, and V91 in M2 are affected by bound ion identity and methyl NOESY spectra reveal that the I88 side-chain conformation switches between Na⁺ and K⁺.

Na⁺ enhances ms timescale dynamics in the SF. We noticed broadening of several NaK methyl resonances, including I84, I88, and I95 on M2, as well as V64 in the SF, both in the presence of K⁺ and Na⁺. Such line broadening can be indicative of ms-timescale conformational exchange, hence ^{13}C Multiple-Quantum (MQ) CPMG experiments were performed to further characterize these potential dynamics[37]. Exchange contributions to the MQ relaxation rates (R_{ex}) are plotted on the NaK structure in Fig. 6a (R_{ex} values and their associated errors can be found in Supplementary Data 3). In K⁺ residues with the highest R_{ex} values indicative of ms-timescale exchange, are localized to the hinge and base of the SF, including I88, L90, and V91 on M2 as well as L35 on M1, V58 in the P helix, and V64 Cγ2 in the SF. More quantitative analysis of exchange rates and populations was hindered by the relatively small size of the exchange contribution for these residues (~4–5 Hz at 800 MHz), which would become even smaller at lower fields, along with the concomitant decrease in signal to noise. However, the fact that the majority of residues with significant R_{ex} contributions are found at the hinge and base of the SF further supports the notion that coupling between the SF and M2 is inherent to NaK and is mediated by the SF-hinge interface.

Surprisingly, CPMG experiments collected for NaK in the presence of Na⁺ revealed a marked increase in R_{ex} for V64 Cγ1 (none to ~15 Hz) and Cγ2 (~4 to ~16 Hz), as well as V59 Cγ2 (~2 to ~4 Hz) (Fig. 6b). Other hinge residues display slightly lower R_{ex} in Na⁺ than K⁺; however, it is difficult to interpret these small differences due to the lower S/N in the Na⁺ dataset. Because V64 is an ion-coordinating residue, a second ^{13}C MQ CPMG data was collected at 600 MHz along with ^{1}H Single Quantum (SQ) CPMG datasets at 900 and 600 MHz for the Na⁺ sample to attempt to quantify the exchange rate[37,38]. Unfortunately, interfering signals from residually protonated DMPC present in the bicelle prevented accurate extraction of V64 peak intensities in some spectra. The ^{1}H SQ CPMG experiment did, however, reveal significant ^{1}H R_{ex} for L48 Hδ atoms that point behind the SF. Global fitting was performed for V64 and V59 ^{13}C MQ and L48 ^{1}H SQ data to extract an estimate for the rate constant for chemical exchange in the SF, k_{ex} (assuming two-state exchange). Satisfactory fits could not be obtained when V64, V59, and L48 were fit globally, likely reflecting multistate exchange as suggested by the three resolved amide resonances for some residues in this region. However, pairwise fitting of V64 and V59 MQ data or V59 MQ and L48 SQ was successful, yielding $k_{ex} = 390 \pm 47$ s⁻¹ and $k_{ex} = 356 \pm 67$ s⁻¹, respectively (Supplementary Fig. 5). Due to the small number of methyl groups and lack of clear evidence to support two-state exchange, we did not attempt to extract populations. In summary, residues in the SF, especially ion-coordinating residue V64, are seen to undergo enhanced chemical exchange in the presence of 600 mM Na⁺ as opposed to 100 mM K⁺, with a timescale of approximately 350 s⁻¹ in Na⁺.

Discussion

There is mounting evidence that multiple SF conformations are needed for non-selective conduction in certain ion channels[13,39]. Additionally, while SF-inner gate coupling has been demonstrated for some K⁺ channels[19,22,23], questions remain regarding the generality of this type of coupling across other channel families. In the present study, we utilized the non-selective, prokaryotic ion channel NaK to characterize how the SF structure and dynamics respond to the identity of the ion occupying the SF and how any changes are allosterically communicated to other parts of the channel.

We found that the NaK SF is structurally labile and that the SF conformation is ion-dependent (Fig. 3). This notion is in contrast

to crystal structures of NaK where the SF structure is identical in 500 mM Na$^+$ and 100 mM K$^+$ and in agreement with a prior ssNMR study of NaK where V64 and G65 had ion-dependent chemical shifts (Fig. 1)[13,34,40]. Our observation of enhanced ps-ns dynamics for D66-S70 also explains the difficulty of observing this region in ssNMR spectra. In line with the backbone flexibility, we observe extensive backbone CSPs in this region between K$^+$ and Na$^+$-bound samples. Observed CSPs are in accord with two recent structures of NaK solubilized in DM – a microED structure solved in Na$^+$ (6CPV [https://doi.org/10.2210/pdb6CPV/pdb])[14] and a new X-ray structure solved in mixed ion conditions (6V8Y [https://doi.org/10.2210/pdb6V8Y/pdb])[15]. In both structures, N68 adopts alternative conformations that alter backbone ϕ and ψ angles for N68 and F69, and slightly reorient the F69 sidechain. Accordingly, we see large CSPs for HN, Cα, and C' for both N68 and F69, where the perturbations to Cα are the largest for all Cα's from residues 65-70 in our samples (Fig. 3). The carbonyl group for D66 is also reoriented in one protomer, largely affecting the conformation of D66 C' and G67 HN[15]. Again, we see large perturbations to both D66 C' and G67 HN chemical shifts. Thus, our CSP data collected in a lipidic environment are consistent with the perturbations to the canonical SF structure observed in detergent-solubilized structures of NaK.

The dynamic nature of the NaK SF has important implications for the permeation and non-selectivity mechanisms of NaK and other non-selective ion channels. Our relaxation data are in accord with MD simulations of the non-selective channels NaK, NaK2CNG, and TRPV1 showing that these SFs are highly dynamic[13,39,41–43]. Interestingly, the TRPV1 SF was reported to adopt different structural states during K$^+$ and Na$^+$ permeation[39]. The activated state structure of the TRPV1 SF (3J5Q [https://doi.org/10.2210/pdb3J5Q/pdb]) was stable during K$^+$ permeation, but an asymmetric deformation occurred during Na$^+$ permeation as a result of Na$^+$ binding to an aspartate adjacent to the conduction path during the simulation. Analogously, a putative Na$^+$ binding site behind the SF was proposed to stabilize the alternate conformation of D66 seen in the recently published 6V8Y [https://doi.org/10.2210/pdb6V8Y/pdb] structure of NaK[15]. The break in SF symmetry in TRPV1 is also is reminiscent of results for NaK, where Na$^+$ permeation only occurred in forced asymmetric states[13], although Na$^+$ could permeate the TRPV1 SF in both symmetric and asymmetric conformations[39]. The appearance of multiple states for several SF residues in the presence of Na$^+$ could indicate a break in SF symmetry in our NMR samples and support the notion that Na$^+$ may permeate NaK in an asymmetric filter conformation.

Considering these results for TRPV1 and NaK, it appears that conformational flexibility in the SF is important for non-selective conduction, especially in the case of the Na$^+$. SF plasticity may allow both K$^+$ and Na$^+$ to permeate efficiently in different conformations. For example, SF flexibility may allow Na$^+$ to permeate in a hydrated or partially hydrated state, as suggested by simulations of NaK2CNG-N[11]. Because dehydration is more unfavorable for Na$^+$ than K$^+$, allowing Na$^+$ to permeate while hydrated may contribute to non-selective conductance. This notion is in accord with different MD studies showing that selectivity is generally decreased as ion hydration in the SF increases[11,43]. On the other hand, in recent structures of human CNGA1, the SF structure was unchanged over a range of ionic conditions[44]. It is possible that the reported structures do not capture all states necessary for permeation, as was the case with NaK. Alternatively, it may be that since the CNGA1 SF is wider than in NaK, hydrated ions can permeate without any structural change. A similar hypothesis has been proposed for several TRP channels that display wide SF openings even in closed states of channel[7]. Other non-selective channels with available structures, such as TAX-4[45,46] or HCN1[47], were solved in a single ionic condition, limiting insight into how the SF adapts to different types of ions. In any case, our data demonstrate significant dynamics on multiple timescales within the NaK SF, supporting the notion that for non-selective channels with a narrow pore, such as NaK, the flexibility of the SF is required to allow conduction of both K$^+$ and Na$^+$.

We observed a Na$^+$-promoted increase in ms-timescale conformational exchange for L48, V59, and V64, where the increase in R$_{ex}$ for V64 was especially large (Fig. 6, S5). This result is intriguing because the analogous residue in MthK[22,48] (V60) and KcsA[17,20,49] (V76) has been reported to flip such that the ion-coordinating carbonyl group points away from the conduction path. Moreover, the E71A mutant of KcsA crystallized in the flipped conformation in high Na$^+$ and was less K$^+$-selective than WT KcsA, suggesting that carbonyl flipping could promote non-selectivity[20]. A previous study of NaK proposed that carbonyl flipping occurs at residue T62, which could in principle cause exchange-induced line-broadening of V64; however, our NMR data cannot distinguish between these possibilities[13].

We found that not only is the NaK SF structure ion-dependent, but that the structural perturbation extends to M2 via I88 (Fig. 3, Fig. 5). Although methyl NOESY data did not reveal a large-scale conformational change in M2, CSPs observed below the hinge, near the proposed bundle crossing suggest small structural perturbation extend down M2 from the hinge. Interestingly, the recent 6V8Y [https://doi.org/10.2210/pdb6V8Y/pdb] structure of NaK showed M2 adopting slightly different conformations in each of two protomers in the asymmetric unit[15] and our ^{15}N relaxation data shows that M2 becomes progressively more flexible after residue ~97 (Fig. 2). Together, these data show that M2 has some degree of conformational flexibility and supports the notion that environmental factors, such as bound ion identity, could influence the structural ensemble of M2.

Significantly, we observed a change in side-chain conformation for I88 between K$^+$ and Na$^+$ conditions. I88 is analogous to I84 in MthK and I100 in KcsA, both of which have been implicated in mediating allosteric coupling between the SF and intracellular gate for these channels (Fig. 1)[19,22–24]. For MthK and KcsA, the inter-gate coupling is thought to be important in both activation and inactivation[17,18,21,22,25]. The activating stimulus for NaK is not currently known, nor is it known whether or not NaK undergoes inactivation in a manner similar to KcsA. Thus, we cannot say for certain which processes are influenced by SF-hinge coupling in NaK; however, our data suggests that allosteric coupling extends to NaK and supports a broader mechanism of allosteric regulation for channel pore domains, with a key role for the residue in the structurally-homologous position to I88 in NaK.

In conclusion, we have shown that the NaK SF displays a large degree of structural plasticity on multiple timescales. We find the SF exhibits strong dynamics on the ps-ns timescale as well as the ability to adopt multiple ion-dependent states on a slower timescale. CSP data indicate that the slower, ion-dependent conformational change occurs between residues 65–70. These observations are in keeping with results from other non-selective channels showing that multiple SF conformations contribute to non-selective conduction. We also identify a residue located at the M2 hinge in NaK, I88, that is likely responsible for coupling the SF conformation to the inner gate. The analogous residue has been implicated in allosteric coupling in structurally related channels, suggesting that this mechanism of coupling may be quite general.

Methods

Protein expression, purification, and reconstitution. A NaK construct lacking the first 18 residues was used for this study. This construct is very similar to NaKΔ19, which has been extensively characterized by X-ray crystallography and NMR previously[28,36]. Growth and expression of isotopically labeled NaK was carried out as previously described[28]. For ^{15}N relaxation experiments, uniform ^{15}N, ^{2}H labeling was achieved through the use of M9 minimal media supplemented with 1 g/L $^{15}NH_4Cl$, 4 g/L ^{13}C, ^{2}H glucose, and 0.5 g/L ^{15}N, ^{2}H isogro (Sigma-Aldrich) in D_2O. The same isotopically labeled compounds were used to produce ^{13}C-$^{1}H_3$ ILV labeled samples, but the amount of ^{15}N, ^{2}H isogro was reduced to 0.25 g/L and ~140 mg/L 2-keto-3-(methyl-d_3)-butyric acid-4-^{13}C, 3-d, and ~70 mg/L 2-ketobutyric acid-4-^{13}C,3,3-d_2 were added ~30 mins prior to induction.

An SDS-mediated refolding protocol was used for preparing ^{15}N relaxation samples in Na^+ and K^+. This protocol was inspired by other membrane protein refolding studies, where refolding from the SDS-solubilized state has proven fruitful for α-helical membrane proteins[50]. Cells were lysed by sonication in lysis buffer (300 mM NaCl, 2.5 mM MgSO$_4$, 20 mM Tris pH 7.5, DNase, 1 μg/mL pepstatin, 10 μM leupeptin, 100 μM PMSF) with 250 mM sucrose and 1 mg/mL lysozyme. The membrane fraction was isolated by centrifugation at 30,000 x g for 1 hour. The membrane fraction was then resuspended in lysis buffer + 0.5% SDS and allowed to rotate overnight to solubilize and to allow for back-exchange of deuterons to protons at exchangeable sites. Solubilized NaK was then purified via IMAC using Talon cobalt affinity resin (Clontech). For the K^+ sample, the resin was equilibrated with Buffer A1 (300 mM NaCl, 5 mM DM (decyl maltoside, Anatrace), 20 mM Tris pH 8). NaK was then incubated with the resin for 20–30 mins before collecting the flow-through and washing with Buffer A1. The resin was then washed with Buffer A2 (100 mM NaCl, 200 mM KCl, 5 mM DM, 20 mM Tris pH 8) and Buffer B (Buffer A2 + 5 mM imidazole). The resin was then incubated with Buffer C (Buffer A2 + 300 mM imidazole) for 20–30 mins and the elution was collected. For the Na^+ sample, the same process was used, but the wash with Buffer A2 was replaced by an additional wash with Buffer A1 and Buffers B and C were prepared using Buffer A1. Elutions were concentrated to 0.5 mL and loaded on a Superdex 200 column pre-equilibrated with FPLC buffer. For the K^+ sample, the FPLC buffer consisted of 100 mM MOPS, 200 mM K^+, 5 mM DM pH 7. For the Na^+ sample, FPLC buffer consisted of 50 mM MOPS, 600 mM NaCl, 5 mM DM pH 7. Subsequently, FPLC fractions were evaluated using SDS-PAGE and selected fractions were pooled and incubated with thrombin to cleave the His-tag. Cleavage was monitored by SDS-PAGE.

Reconstitution into $q = 0.33$ DMPC/DHPC bicelles was performed using our previously published protocol with a few alterations[28,51]. DMPC powder (1,2-dimyristoyl-sn-glycero-3-phosphocholine, Avanti Polar Lipids) hydrated with NMR buffer (for K^+ − 100 mM MOPS, 100 mM K^+, pH 7; for Na^+ − 50 mM MOPS, 600 mM Na^+, pH 7) at 20 mg/mL was bath sonicated for <1 min, incubated at ~40 °C for 1 hour then bath sonicated again for 5 min. NMR buffer + 100 mM DM was then added to the DMPC to a final DM concentration of 10 mM and allowed to incubate for 15 mins, after which the lipid was incubated with the pooled NaK FPLC fractions for 30 mins. To remove the detergent and form proteoliposomes, one aliquot of Amberlite XAD-2 (BioRad) was added and allowed to incubate for 1 hour, followed by the addition of another aliquot and overnight incubation. The following day, a final aliquot was added and allowed to incubate for 1 hour. The total amount of Amberlite XAD-2 used to remove detergent was equal to 90 mg Amberlite per mg of DM in the sample. NaK proteoliposomes were then collected and pelleted by ultracentrifugation at 150,000 x g for 2 h at 6 °C. The pellet was solubilized using DHPC (1,2-dihexanoyl-sn-glycero-3-phosphocholine, Avanti Polar Lipids) dissolved in NMR buffer at a molar ratio of 3:1 relative to DMPC. The sample was then subjected to four freeze-thaw cycles to produce homogenous bicelles. The Na^+ sample was reconstituted using a molar ratio DMPC:NaK monomer of 95:1 while the K^+ sample was reconstituted using a molar ratio DMPC:NaK monomer of 60:1.

Other NaK samples were prepared in a similar fashion; however, they were solubilized using lysis buffer + 20 mM DM rather than SDS. The samples were allowed to solubilize overnight before IMAC. For Na^+ samples, IMAC was performed as described above. For K^+, the initial wash with Buffer A1 was skipped, but was otherwise performed in the same manner. After IMAC, imidazole was removed using a PD10 desalting column (GE Healthcare) equilibrated with Buffer A1 for Na^+ or Buffer A2 for K^+. Samples were then incubated overnight with thrombin to cleave the His-tag. Samples were further purified by gel filtration chromatography as described above.

Reconstitution was performed nearly as described above for ^{15}N, ^{2}H labeled samples, but with slight alterations for methyl labeled samples. d54-DMPC (Avanti Polar Lipids) was used for methyl labeled samples, where preparation and proteoliposome formation was carried out as above. An aliquot of d22-DHPC (Avanti Polar Lipids) stored in chloroform was dried and then washed three times with pentane before lyophilizing overnight. The next day, the dried d22-DHPC was dissolved in either K^+ or Na^+ NMR buffer and used to solubilize proteoliposomes as described above. Lipid:protein ratios used for reconstitution of non-SDS samples ranged from 60:1-50:1 DMPC:NaK monomer.

NMR Spectroscopy. NMR samples contained 0.5–1.4 mM NaK solubilized in $q = 0.33$ DMPC/DHPC bicelles in buffer containing 50–100 mM MOPS, pH 7 and

100 mM K^+ or 600 mM Na^+ and either 5–10% D_2O for amide-based experiments or 100% D_2O for methyl experiments. Samples in Na^+ were loaded into salt-tolerant Shigemi tubes designed for high salt samples (Shigemi). Our published[28] ^{1}H-^{15}N assignments of NaK in 100 mM K^+ at 60 °C were transferred to 40 °C for the K^+-bound sample using an NMR temperature titration. Assignments for the K^+-bound sample at 40 °C were then transferred to the Na^+-bound sample and confirmed using TROSY-based HNCO and HNCA backbone-walk experiments. All Bruker spectrometers employed in this study used Topspin version 3.5pl7 and all Varian spectrometers used vnmrj version 4.2. TROSY-based HSQC, HNCA, and HNCO spectra were collected at 40 °C on Bruker Avance III NMR spectrometers operating at 750 and 600 MHz (^{1}H) and equipped with cryogenic probes. Three-dimensional spectra were acquired with non-uniform sampling (NUS) using 30-35% sampling rates and reconstructed using the SMILE algorithm (version 1.1) implemented in nmrPipe[52]. ^{1}H-^{13}C HMQC spectra were obtained on an 800 MHz (^{1}H) Varian VNMRS spectrometer equipped with a cryogenic probe. All spectra are referenced using DSS. Amide and methyl chemical shift perturbations (CSPs) were calculated using the formula, $CSP = [\Delta\delta_H^2 + (W*\Delta\delta_{N/C})^2]^{0.5}$ where $\Delta\delta$ is the difference in chemical shift for a given residue between K^+ and Na^+ preferred states and is W a chemical shift weighting factor ($W_N = |\gamma_N/\gamma_H| = 0.101$, $W_C = |\gamma_C/\gamma_H| = 0.251$). Values of $\Delta\delta$ for Cα and C' are presented unweighted. Note that amide CSPs were calculated on SDS back-exchanged spectra, while backbone C' and Cα $\Delta\delta$ were calculated from 3D spectra obtained without SDS back-exchange, resulting in lower sequence coverage.

TROSY ^{15}N R_1, $R_{1\rho}$, and {^1H}-^{15}N NOE experiments[31] were recorded at 40 °C (calibrated using ethylene glycol) on a 750 MHz Bruker Avance III HD spectrometer equipped with a cryogenic probe. The number of scans was adjusted for each experiment in order to obtain satisfactory signal to noise. R_1 and $R_{1\rho}$ values were measured using 5 relaxation delays. R_1 experiments on the Na^+ sample were recorded using a recycle delay of 2 s and relaxation delays of 0, 0.4,1.4, 2.4, and 3.6 s. For the K^+ sample, the recycle delay was set to 2.5 s and relaxation delays were 0.08, 0.4, 1.2, 2, and 4 s. For $R_{1\rho}$ experiments on both samples the recycle delay was set to 2.5 s and relaxation delays were set to 2, 8, 12, 18, and 25 ms. The spin-lock field strength was set to 1923 Hz in both cases. The {^1H}–^{15}N NOE experiment utilized a 15 s proton saturation time for the NOE experiment with an equivalent recovery delay in the reference experiment, each preceded by an additional recovery time of 1 s. The total experimental time for R_1 and $R_{1\rho}$ experiments was approximately 3 days each, while the NOE experiment took ~7 days.

All spectra were processed using nmrPipe version 9.0[53] and visualized using ccpNmr analysis version 2.4.2[54]. Peak heights and the standard deviation of the base plane noise (taken to be the error in the peak height) were extracted using ccpNmr analysis. If the error in peak height was less than 2% based on the signal to noise, an error of 2% was assumed. R_1 and $R_{1\rho}$ values were determined by fitting the data to the single exponential decay I_0e^{-Rt} using home-written Python scripts utilizing the *scipy.optimize.curve_fit* function. Errors were determined as the standard deviation of 500 Monte Carlo simulations, where the peak height is taken from a Gaussian distribution centered on the measured value and the width is defined by the error in peak height as determined by the S/N of the experiment. All curves were well described by the single exponential, with no statistical justification for pursuing more complex models. $R_{1\rho}$ values were converted to R_2 using the formula $R_2 = R_{1\rho}/\sin^2\theta - R_1/\tan^2\theta$, where $\theta = \tan^{-1}(\omega/\Omega)$, ω is the spin-lock field strength, and Ω the offset from the ^{15}N carrier frequency. {^1H}–^{15}N NOE values were calculated as the ratio of peak heights in experiments with and without ^1H saturation. The error in the NOE was calculated using standard error propagation.

3D CCH HMCQ-NOESY-HMQC spectra[55] were obtained for samples in K^+ and Na^+ on an 800 MHz Varian spectrometer. Both spectra were collected with 64 (8 ms) x 96 (11 ms) x 1024 (^{13}C–^{13}C–^{1}H) complex points sampled at a 35% NUS rate for Na^+ and 40% for K^+ and reconstructed using SMILE[52]. The NOE mixing time was set to 200 ms and the recycle delay was set to 1 s for both samples. The total experimental time for both samples was ~7 days.

CPMG experiments were obtained on ILV labeled NaK samples in 100 mM K^+ and 600 mM Na^+ purified as described above. All experiments were collected at 40 °C (calibrated using ethylene glycol). ^{13}C MQ and ^1H SQ experiments were performed using pulse sequences reported by Kay and colleagues[37,38]. For the K^+ sample, a ^{13}C MQ dataset was recorded on 800 MHz Varian spectrometer using $T_{relax} = 20$ ms and ν_{CPMG} values of 50, 100, 200 (x2), 250, 300, 350, 400, 500, 600 (x2), 800, and 1000 Hz. For the Na^+ sample, ^{13}C MQ datasets were recorded on 800 and 600 MHz Varian spectrometers using $T_{relax} = 30$ ms and ν_{CPMG} values of 33.33, 66.67, 100, 133.33 (x2), 166.67, 200, 233.33, 266.67 (x2), 300, 333.33, 366.67, 400, 466.67, 533.33 (x2), 600, 666.67, 800, 900, and 1000 Hz. ^1H SQ datasets for the Na^+ sample were collected on Bruker spectrometers operating at 900 and 600 MHz using $T_{relax} = 20$ ms and ν_{CPMG} values of 50, 100 (x2), 150, 200, 250, 300, 350, 400 (x2), 450, 500, 600 (x2), 700, 800, 900, and 1000 Hz. The error in $R_{2,eff}$ values were determined from replicated data points. R_{ex} values were calculated as $I_{(\nu CPMG = 50\,Hz)} - I_{(\nu CPMG = 1000\,Hz)}$ for K^+ and $I_{(\nu CPMG = 33.33\,Hz)} - I_{(\nu CPMG = 1000\,Hz)}$ for Na^+. The error in R_{ex} was calculated using standard error propagation. We note that because R_{ex} was determined by simply subtracting the calculated $R_{2,eff}$ values for the lowest and highest ν_{CPMG} values, as opposed to obtaining R_{ex} by fitting the entire dispersion curve, the error in R_{ex} is likely underestimated for a majority of residues. The Na^+ ^{13}C MQ and ^1H SQ dispersion curves were fit using ChemEx version 2019.1.0[38,56].

Assignment of methyl resonances. In total, four separate samples were used to assign ILV methyl groups. One sample utilized the full-length NaK channel (FL-NaK) while the other three utilized NaKΔ18. These samples were expressed and purified as described above. The FL-NaK sample was produced as described above for ILV labeled samples, except 2-Keto-3-(methyl-d_3)-butyric acid-1,2,3,4-$^{13}C_4$, 3-d was used as a precursor to label valines and leucines. Three 3D COSY[57] experiments were recorded ($1024 \times 64 \times 48$ points, 8 scans, 47% non-uniform sampling), each using either one, two, or three transfer steps, on an 800 MHz Varian spectrometer. The experiment allowed us to obtain correlations between valine Cγ, Cβ, and Cα, as well as leucine Cδ and Cβ resonances. However, we could not obtain any Leu Cα resonances, presumably due to R_2 relaxation during the 3-step transfer. All subsequent methyl assignment experiments were performed using NaK constructs lacking the M0 helix.

We have further produced a sample where NaK was expressed in D_2O with ^{13}C, ^1H glucose as a carbon source and recorded 3D C-TOCSY-CHD$_2$-HSQC experiment, as previously described[58] (512x64x34 points, 32 scans, 47% non-uniform sampling). This experiment revealed correlations between all isoleucine, valine, and leucine aliphatic carbon resonances.

Both of these experiments allowed us to determine which valine and leucine pro-S and pro-R methyl resonances belong to the same residue, as well as to distinguish valine and leucine cross-peaks in the ^1H-^{13}C HMQC spectrum. Furthermore, the comparison of COSY and TOCSY experiments with data from HNCACB and HNCA experiments allowed us to correlate leucine and isoleucine Cδ and valine Cγ resonances to HN, and thus determine the identity of the residue giving the origin to particular methyl group cross-peaks. Using these two experiments we could unambiguously assign all isoleucine, 50% of valine, and 20% of leucine resonances. We could not unambiguously assign the remaining residues either due to the lack of resolution in our 3D spectra, or the lack of Cβ cross-peaks in the HNCACB experiment.

To obtain the full assignment, we have recorded the 3D CCH HMQC-NOESY-HMQC experiment displaying correlations between spatially proximal methyl groups, as described above, and used MAGMA version 1.2.3[59] without using the restraints from COSY and TOCSY experiments, except differentiating leucine and valine cross-peaks. The 3E8H [https://doi.org/10.2210/pdb3E8H/pdb] NaK crystal structure was used to generate the connectivity graph. MAGMA produced confident assignments for 20 out of 30 assignable residues. Two residues, L48 and V45 are too far away from any other methyl group, and thus were not included in the calculation. Comparison of data obtained with COSY and TOCSY experiments were in an excellent agreement, and the remaining ambiguous assignments proposed by MAGMA could be easily resolved.

Lastly, we performed a 3D ^1H-NOESY-^1H,^{15}N-HSQC experiment on the same sample as was used to record the 3D CCH HMQC-NOESY-HMQC experiment to validate our assignment. The experiment was performed with 46% non-uniform sampling, with 1024x96x40 points, 32 scans, 140 ms mixing time. This experiment reveals correlations between nearby methyl and amide groups. The experiment was in complete agreement with our methyl assignment data.

Data availability

Backbone amide and ILV methyl chemical shifts in K^+ and Na^+ are available at BMRB under deposition numbers 51063 [https://doi.org/10.13018/BMR51063] and 51064 [https://doi.org/10.13018/BMR51064], respectively. Raw NMR data is deposited in BMRBig [https://bmrbig.org/] with deposition IDs bmrbig25 and bmrbig26 for K^+ and Na^+ data, respectively. ^{15}N relaxation parameters, chemical shift perturbation values, and CPMG R_{ex} values are provided in the Supplementary Data 1-3. This study utilized PDB accession codes 3E8H [https://doi.org/10.2210/pdb3E8H/pdb], 3E83 [https://doi.org/10.2210/pdb3E83/pdb], 6CPV [https://doi.org/10.2210/pdb6CPV/pdb], 6V8Y [https://doi.org/10.2210/pdb6V8Y/pdb], 3LDC [https://doi.org/10.2210/pdb3LDC/pdb], 1K4C [https://doi.org/10.2210/pdb1K4C/pdb], and 3J5Q [https://doi.org/10.2210/pdb3J5Q/pdb].

References

1. Doyle, D. A. et al. The structure of the potassium channel: molecular basis of K+ conduction and selectivity. *Science* **280**, 69–77 (1998).
2. Zhou, Y., Morais-Cabral, J. H., Kaufman, A. & MacKinnon, R. Chemistry of ion coordination and hydration revealed by a K+ channel–Fab complex at 2.0 Å resolution. *Nature* **414**, 43–48 (2001).
3. Ye, S., Li, Y. & Jiang, Y. Novel insights into K+ selectivity from high-resolution structures of an open K+ channel pore. *Nat. Struct. Mol. Biol.* **17**, 1019–1023 (2010).
4. Kuang, Q., Purhonen, P. & Hebert, H. Structure of potassium channels. *Cell. Mol. Life Sci.* **72**, 3677–3693 (2015).
5. Kim, D. M. & Nimigean, C. M. Voltage-gated potassium channels: a structural examination of selectivity and gating. *Cold Spring Harb. Perspect. Biol.* **8**, a029231 (2016).
6. James, Z. M. & Zagotta, W. N. Structural insights into the mechanisms of CNBD channel function. *J. Gen. Physiol.* **150**, 225–244 (2018).
7. Cao, E. Structural mechanisms of transient receptor potential ion channels. *Journal of General Physiology* **152**, (2020).
8. Alam, A. & Jiang, Y. High-resolution structure of the open NaK channel. *Nat. Struct. Mol. Biol.* **16**, 30–34 (2009).
9. Alam, A. & Jiang, Y. Structural analysis of ion selectivity in the NaK channel. *Nat. Struct. Mol. Biol.* **16**, 35–41 (2009).
10. Köpfer, D. A. et al. Ion permeation in K+ channels occurs by direct Coulomb knock-on. *Science* **346**, 352–355 (2014).
11. Kopec, W. et al. Direct knock-on of desolvated ions governs strict ion selectivity in K+ channels. *Nat. Chem.* **10**, 813–820 (2018).
12. Furini, S. & Domene, C. Gating at the selectivity filter of ion channels that conduct Na + and K + ions. *Biophys. J.* **101**, 1623–1631 (2011).
13. Shi, C. et al. A single NaK channel conformation is not enough for non-selective ion conduction. *Nat. Commun.* **9**, 717 (2018).
14. Liu, S. & Gonen, T. MicroED structure of the NaK ion channel reveals a Na+ partition process into the selectivity filter. *Commun. Biol.* **1**, 38 (2018).
15. Roy, R. N. et al. Structural plasticity of the selectivity filter in a nonselective ion channel. *IUCrJ* **8**, 421–430 (2021).
16. Chakrapani, S., Cordero-Morales, J. F. & Perozo, E. A quantitative description of KcsA gating I: macroscopic currents. *J. Gen. Physiol.* **130**, 465–478 (2007).
17. Cordero-Morales, J. F. et al. Molecular determinants of gating at the potassium-channel selectivity filter. *Nat. Struct. Mol. Biol.* **13**, 311–318 (2006).
18. Cuello, L. G., Jogini, V., Cortes, D. M. & Perozo, E. Structural mechanism of C-type inactivation in K+ channels. *Nature* **466**, 203–208 (2010).
19. Cuello, L. G. et al. Structural basis for the coupling between activation and inactivation gates in K+ channels. *Nature* **466**, 272–275 (2010).
20. Cheng, W. W. L., McCoy, J. G., Thompson, A. N., Nichols, C. G. & Nimigean, C. M. Mechanism for selectivity-inactivation coupling in KcsA potassium channels. *Proc. Natl Acad. Sci. USA* **108**, 5272–5277 (2011).
21. Heer, F. T., Posson, D. J., Wojtas-Niziurski, W., Nimigean, C. M. & Bernèche, S. Mechanism of activation at the selectivity filter of the KcsA K+ channel. *Elife* **6**, e25844 (2017).
22. Kopec, W., Rothberg, B. S. & de Groot, B. L. Molecular mechanism of a potassium channel gating through activation gate-selectivity filter coupling. *Nat. Commun.* **10**, 1–15 (2019).
23. Wylie, B. J., Bhate, M. P. & McDermott, A. E. Transmembrane allosteric coupling of the gates in a potassium channel. *Proc. Natl Acad. Sci. USA* **111**, 185–190 (2014).
24. Xu, Y., Zhang, D., Rogawski, R., Nimigean, C. M. & McDermott, A. E. Identifying coupled clusters of allostery participants through chemical shift perturbations. *Proc. Natl Acad. Sci. USA* **116**, 2078–2085 (2019).
25. Boiteux, C., Posson, D. J., Allen, T. W. & Nimigean, C. M. Selectivity filter ion binding affinity determines inactivation in a potassium channel. *Proc. Natl Acad. Sci. USA* **117**, 29968–29978 (2020).
26. Amani, R. et al. Conformational changes upon gating of KirBac1.1 into an open-activated state revealed by solid-state NMR and functional assays. *Proc. Natl Acad. Sci. USA* **117**, 2938–2947 (2020).
27. Derebe, M. G. et al. Tuning the ion selectivity of tetrameric cation channels by changing the number of ion binding sites. *Proc. Natl Acad. Sci. USA* **108**, 598–602 (2011).
28. Brettmann, J. B., Urusova, D., Tonelli, M., Silva, J. R. & Henzler-Wildman, K. A. Role of protein dynamics in ion selectivity and allosteric coupling in the NaK channel. *Proc. Natl Acad. Sci. USA* **112**, 15366–15371 (2015).
29. Liu, S. & Lockless, S. W. Equilibrium selectivity alone does not create K +-selective ion conduction in K+ channels. *Nat. Commun.* **4**, 2746 (2013).
30. Shi, C. et al. A single NaK channel conformation is not enough for non-selective ion conduction. *Nat. Commun.* **9**, 717 (2018).
31. Lakomek, N. A., Ying, J. & Bax, A. Measurement of 15N relaxation rates in perdeuterated proteins by TROSY-based methods. *J. Biomol. NMR* **53**, 209–221 (2012).
32. Jarymowycz, V. A. & Stone, M. J. Fast time scale dynamics of protein backbones: NMR relaxation methods, applications, and functional consequences. *Chem. Rev.* **106**, 1624–1671 (2006).
33. Chill, J. H., Louis, J. M., Baber, J. L. & Bax, A. Measurement of 15N relaxation in the detergent-solubilized tetrameric KcsA potassium channel. *J. Biomol. NMR* **36**, 123–136 (2006).
34. Hendriks, K., Öster, C., Shi, C., Sun, H. & Lange, A. Sodium ions do not stabilize the selectivity filter of a potassium channel. *J. Mol. Biol.* 167091 (2021). https://doi.org/10.1016/j.jmb.2021.167091
35. Shi, N., Ye, S., Alam, A., Chen, L. & Jiang, Y. Atomic structure of a Na+- and K+-conducting channel. *Nature* **440**, 570–574 (2006).

36. Alam, A. & Jiang, Y. High-resolution structure of the open NaK channel. *Nat. Struct. Mol. Biol.* **16**, 30–34 (2009).

37. Korzhnev, D. M., Kloiber, K., Kanelis, V., Tugarinov, V. & Kay, L. E. Probing slow dynamics in high molecular weight proteins by methyl-TROSY NMR spectroscopy: application to a 723-residue enzyme. *J. Am. Chem. Soc.* **126**, 3964–3973 (2004).

38. Yuwen, T., Huang, R., Vallurupalli, P. & Kay, L. E. A methyl-TROSY-based 1H relaxation dispersion experiment for studies of conformational exchange in high molecular weight. *Proteins Angew. Chem. - Int. Ed.* **58**, 6250–6254 (2019).

39. Darré, L., Furini, S. & Domene, C. Permeation and dynamics of an open-activated TRPV1 channel. *J. Mol. Biol.* **427**, 537–549 (2015).

40. Alam, A. & Jiang, Y. Structural analysis of ion selectivity in the NaK channel. *Nat. Struct. Mol. Biol.* **16**, 35–41 (2009).

41. Jorgensen, C., Furini, S. & Domene, C. Energetics of ion permeation in an open-activated TRPV1 channel. *Biophys. J.* **111**, 1214–1222 (2016).

42. Napolitano, L. M. R. et al. A structural, functional, and computational analysis suggests pore flexibility as the base for the poor selectivity of CNG channels. *Proc. Natl Acad. Sci. USA* **112**, E3619–E3628 (2015).

43. Noskov, S. Y. & Roux, B. Importance of hydration and dynamics on the selectivity of the KcsA and NaK channels. *J. Gen. Physiol.* **129**, 135–143 (2007).

44. Xue, J., Han, Y., Zeng, W., Wang, Y. & Jiang, Y. Structural mechanisms of gating and selectivity of human rod CNGA1 channel. *Neuron* **109**, 1302–1313.e4 (2021).

45. Li, M. et al. Structure of a eukaryotic cyclic-nucleotide-gated channel. *Nature* **542**, 60–65 (2017).

46. Zheng, X. et al. Mechanism of ligand activation of a eukaryotic cyclic nucleotide−gated channel. *Nat. Struct. Mol. Biol.* **27**, 625–634 (2020).

47. Lee, C.-H. & MacKinnon, R. Structures of the Human HCN1 Hyperpolarization-Activated Channel. *Cell* **168**, 111–120.e11 (2017).

48. Thomson, A. S. et al. Initial steps of inactivation at the K + channel selectivity filter. *Proc. Natl Acad. Sci. USA* **111**, E1713–E1722 (2014).

49. Kratochvil, H. T. et al. Instantaneous ion configurations in the K+ ion channel selectivity filter revealed by 2D IR spectroscopy. *Science* **353**, 1040–1044 (2016).

50. Popot, J.-L. Folding membrane proteins in vitro: a table and some comments. *Arch. Biochem. Biophys.* **564**, 314–326 (2014).

51. Morrison, E. A. & Henzler-Wildman, K. A. Reconstitution of integral membrane proteins into isotropic bicelles with improved sample stability and expanded lipid composition profile. *Biochim. Biophys. Acta - Biomembr.* **1818**, 814–820 (2012).

52. Ying, J., Delaglio, F., Torchia, D. A. & Bax, A. Sparse multidimensional iterative lineshape-enhanced (SMILE) reconstruction of both non-uniformly sampled and conventional NMR data. *J. Biomol. NMR* **68**, 101–118 (2017).

53. Delaglio, F. et al. NMRPipe: A multidimensional spectral processing system based on UNIX pipes. *J. Biomol. NMR* **6**, 277–293 (1995).

54. Vranken, W. F. et al. The CCPN data model for NMR spectroscopy: development of a software pipeline. *Proteins Struct. Funct. Genet* **59**, 687–696 (2005).

55. Schanda, P., Kupĉe, E. & Brutscher, B. SOFAST-HMQC experiments for recording two-dimensional deteronuclear correlation spectra of proteins within a few seconds. *J. Biomol. NMR* **33**, 199–211 (2005).

56. Vallurupalli, P., Bouvignies, G. & Kay, L. E. Studying 'invisible' excited protein states in slow exchange with a major state conformation. *J. Am. Chem. Soc.* **134**, 8148–8161 (2012).

57. Tugarinov, V. & Kay, L. E. Ile, Leu, and Val methyl assignments of the 723-residue malate synthase G using a new labeling strategy and novel NMR methods. *J. Am. Chem. Soc.* **125**, 13868–13878 (2003).

58. Otten, R., Chu, B., Krewulak, K. D., Vogel, H. J. & Mulder, F. A. A. Comprehensive and cost-effective NMR spectroscopy of methyl groups in large proteins. *J. Am. Chem. Soc.* **132**, 2952–2960 (2010).

59. Pritišanac, I. et al. Automatic assignment of Methyl-NMR spectra of supramolecular machines using graph theory. *J. Am. Chem. Soc.* **139**, 9523–9533 (2017).

Acknowledgements

Author contributions

A.L. prepared NaK samples, collected and analyzed NMR data, wrote the original manuscript, and revised the manuscript. V.K. prepared NaK samples, performed methyl group assignments, and revised the manuscript. M.T. assisted in NMR data collection and revised the manuscript. K.H.W. supervised the project, acquired funding, and revised the manuscript.

Competing interests

The authors declare no competing interests.

Additional information

Supplementary information The online version contains supplementary material available at https://doi.org/10.1038/s41467-021-26538-8.

Correspondence and requests for materials should be addressed to Katherine Henzler-Wildman.

Peer review information *Nature Communications* thanks the anonymous reviewer(s) for their contribution to the peer review of this work.

Reprints and permission information is available at http://www.nature.com/reprints

Publisher's note Springer Nature remains neutral with regard to jurisdictional claims in published maps and institutional affiliations.